Conformational Dependence of the Electronic Properties of $[Fe(SCH_3)_4]^{-,2-}$

John B. Koerner and Toshiko Ichiye*

Departments of Biochemistry/Biophysics and of Chemistry, Washington State University, Pullman, Washington 99164-4660

Received: November 22, 1996[⊗]

The electronic properties of $[Fe(SCH_3)_4]^{-,2-}$, a model for the iron−sulfur site in rubredoxin, and the conformational dependence of these properties were investigated with *ab initio* calculations. The calculations were done at the unrestricted Hartree−Fock level with various basis sets, and the effects of electron correlation were tested in some calculations using second-order perturbation theory. The conformational dependence was studied using five conformations of the model complex that differed by rotations about the Fe−S and C−S bonds. Geometry optimizations showed that these bond lengths changed little among the conformations examined, except where steric crowding existed. The atomic spin populations and spin contamination values (S^2) were also homogeneous among the conformations. The relative energies of all but one of the conformations were very small in both the oxidized and reduced states; thus, the total energy changes upon reduction, ΔE_{redox}, of all but one of the conformations were within 30 mV of each other. The exception was about 100 mV less negative than the other four structures and represents a less likely dihedral rotation transition state. More important, the difference of only 30 mV between conformations similar to that of the iron−sulfur site in rubredoxin and in the Holm−Ibers analogue indicates that very little of the 800 mV difference in redox potential between rubredoxin and in the Holm−Ibers analogue can be attributed strictly to conformationally dependent differences in electronic structure. In addition, atom-centered partial charges were determined by Mulliken's method and two different electrostatic potential (ESP) fitting methods: the surface-based geodesic tessellation method and the grid-based CHELPG method. For all three methods, the partial charge distributions showed little conformational dependence. Moreover, the Mulliken charges, which are not subject to the problems of buried atoms associated with ESP methods, indicate very little conformational dependence. The CHELPG partial charges were selected as being the most reasonable for ESP calculations; thus, a geometry-independent set of CHELPG partial charges is proposed.

1. Introduction

Iron−sulfur proteins are ubiquitous electron transfer proteins that are characterized by a redox site containing iron and sulfur. The structures of well over 100 iron−sulfur proteins have been determined by X-ray crystallography,[1] with Fe−S sites ranging from those containing only a single iron [1Fe], which is tetrahedrally coordinated to cysteinyl sulfurs, to those with four irons and four inorganic sulfurs [4Fe−4S], also with the irons coordinated to cysteinyl sulfurs.[1,2] The Fe−S proteins, including those with homologous redox sites, exhibit a broad range of redox potentials and participate in many different metabolic processes. Unraveling the operative mechanism of electron transfer for an Fe−S protein at a molecular level begins with an understanding of the redox site itself, along with a determination of how the protein modulates its electronic properties.

The factors affecting the redox potentials can be conveniently divided into two groups: those intrinsic to the iron−sulfur redox site and those due to the surrounding environment. One of the common features among all of the Fe−S sites are cysteinyl sulfurs that bind the irons to the surrounding protein matrix. The relative proximity of these sulfurs (along with bridging inorganic sulfurs) to the irons of the cluster determines the nature of the ligand field experienced by the irons. This, in turn, dictates the oxidation states available to the metals, an electronic property that ultimately affects the redox potential of the protein. Determining how the geometry affects the intrinsic redox potential will be the main focus of this study.

Experimental research on Fe−S proteins has included determining the factors that contribute to the redox potentials and quantifying the importance of their respective roles. The intrinsic redox potentials of the Fe−S sites have been examined experimentally by synthesizing and analyzing analogues in which the peptide's cysteinyl sulfurs are replaced by model thiolate ligands,[3,4] which exhibit a wide range of dihedral angles associated with the Fe−S bonds. Understanding how the extrinsic environment of the iron−sulfur site contributes to the redox potential is more difficult since it includes contributions due to both the protein matrix and the solvent. Although these effects may also be a function of the dihedral angles associated with the Fe−S bonds,[5] analogues of Fe−S sites[3] and hemes[6] show significant shifts in their redox potentials, depending upon the polarity of the solvent in which the measurement is carried out. Furthermore, the redox potentials exhibited by a protein and its corresponding analogue can be quite different.[3] Experiments that have attempted to measure the respective roles of the protein matrix and solvent on the iron−sulfur site have only been partially fruitful and thus provide an active area of research.[7−11]

Computational studies have also been conducted to examine these factors. For instance, several quantum calculations on Fe−S sites have been performed at various levels to examine the intrinsic contributions to the redox potential. The [1Fe] redox site is particularly well suited for such calculations since it consists of only a single iron ligated to four cysteinyl sulfurs arranged in a tetrahedron around the metal. Early semiempirical calculations on this site indicated dependence of some electronic properties on the geometry, particularly the orientation of C_β, although the geometries tested were extreme.[12] More reasonable

* To whom all correspondence should be addressed. E-mail Ichiye@wsu.edu; FAX (509) 335-9688.

[⊗] Abstract published in *Advance ACS Abstracts,* April 1, 1997.

S1089-5647(96)03897-7 CCC: $14.00

model geometries were proposed later in a Hartree−Fock (HF) study, though only single-point energy calculations were done and the β methyl groups were modeled with hydrogens.[13,14] Nonetheless, the results showed a sensitivity of the orbital energies to the dihedral angles associated with the Fe−S bonds, which was proposed as a mechanism for exerting control over the redox potential of the protein. One of these conformations was examined further by including electron correlation via configuration interaction (CI) calculations, a study which also attempted to include solvation effects.[14] Finally, the electronic structure of the [1Fe] site has been examined using density functional theory (DFT).[15−19] In the most recent of these studies, atom-centered "partial" charges of the [1Fe] site were determined for electrostatic energy calculations based on the electrostatic potential from the DFT calculations. This reaction field was then placed in a continuous dielectric medium to determine the solvation energy, that when added to the ionization potential (IP) gave an estimate of the absolute redox potential of the system. However, the results were not very sensitive to the actual values of the partial charges. Moreover, only one unoptimized experimental geometry for each state was tested.

Computational studies of the role of the protein environment around the [1Fe] site have also been carried out for rubredoxin. This protein has a single [1Fe] site and has a relatively small molecular weight of about 6000. Several high-resolution crystal structures of different homologous forms have been determined.[20−23] Energetic calculations have indicated that the electrostatic potential at the iron due to the protein is a major contributor to the redox potential.[24] Molecular dynamics simulations of an analogue in water[5] and of the protein in its reduced state also surrounded by water,[25] using partial charges on the Fe−S site from the earlier DFT calculations,[18] indicate the close approach of solvent water to the Fe atom. In both cases, the water approached close enough to perturb the electronic charge distribution of the [1Fe] site. To understand the molecular basis for the redox properties of rubredoxin, it is crucial to determine how close water can actually approach the Fe−S site. Since the partial charges of the [1Fe] site determine the trajectory of an approaching water, accurate partial charges calculated at high quantum mechanical levels for use in classical simulations are crucial in determining whether this close water is real or merely a computational artifact.

The dependence of these partial charges on the conformations of the bonds nearest the redox site is an inherent part of this problem. Rotations around the Fe−S and S−C bonds can alter the donor/acceptor properties of the thiolate ligands and thus change the electronic distribution within the redox site. Although in an experimental study of homologous Fe−S proteins differences in structure of the redox site could not account for the observed differences in the redox potentials,[26] to date the extent to which the redox site must be distorted to change the redox potential has not been quantified. Moreover, the degree of solvation of the site is also clearly dependent on these conformational degrees of freedom since the extent to which the iron is exposed to the surrounding environment is contingent on them. For example, although the redox site in rubredoxin compared to that in the Holm−Ibers analogue (Figure 1) has the same [1Fe] core region of iron coordinating to the four sulfurs, the different orientations of atoms beyond the sulfurs can influence the electrostatics both electronically and sterically. Analysis of the electronic structure and the conformational dependence of partial charges of the redox site of these systems in vacuo allows separation of the electronic versus environmental effects.

Conventional *ab initio* studies are appropriate since further studies of the metal site interacting with H_2O can then take advantage of the wealth of existing *ab initio* studies of water, and more importantly, although DFT has been used to study intermolecular complexes, including metal clusters with atoms and molecules,[27] these types of studies are not as well developed as in standard *ab initio* methods. In fact, a recent study of van der Waals complexes using the local density approximation (LDA) even with nonlocal density gradient corrected functionals was not successful for predicting binding[28] although other LDA studies of hydrogen bonding with these corrections have been quite successful.[29] Furthermore, the focus of this study on conformational energies indicates the proper use of HF/MP2 methods since they represent conformational energies of saturated systems, such as rotational barriers in alkanes, quite well. Moreover, comparisons of conventional *ab initio* methods to DFT are important in understanding the relative accuracy of these methods for organometallics in general, and so the recent DFT results[19] make a conventional *ab initio* study timely.

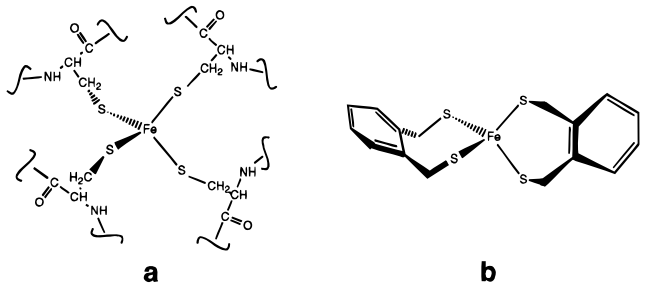

Figure 1. Schematic of the [1Fe] site (a) in the protein rubredoxin and (b) in the Holm−Ibers analogue.

Here, we present a quantum mechanical study of the [1Fe] site, with three major goals in mind. The first goal is to do high-level *ab initio* calculations on the Fe−S site, studying the effects of electron correlation and the size of the basis set on the optimized geometries, energies, and atomic spin populations. These calculations are compared to the recent DFT results.[19] The second goal is to obtain accurate partial charges for molecular dynamics simulations using electrostatic potential (ESP) fitting methods on the best wave function calculated. Again, these partial charges are compared to those in the recent DFT study.[19] The final goal is to study the conformational dependence of the electronic properties of [1Fe], including partial charges and estimated ionization energies, and then infer how they may affect the redox potentials. These conformations are doubly important since they affect the electronic structure at the metal center and also determine the accessibility of the site to portions of the surrounding protein and the solvent. A future study will describe the interaction of the [1Fe] site with water.[30]

2. Computational Methodology

a. Models. The active site of rubredoxin was modeled by an iron atom surrounded by four $(H_3CS)^-$ groups. Previous work indicates that it is necessary and sufficient to model the β positions with methyl groups rather than to terminate with hydrogens.[18] The four methiolate ligands model both the cysteine residues found in the protein and thiolate ligands found in the experimental analogues. The orientation of these ligands can be designated by first defining a face of the tetrahedron formed by the sulfurs. For example, the face made up of S_2, S_3, and S_4 can be designated S_2:S_3:S_4 (Figure 2). Then, each of the carbons in the molecule can be oriented either cis or trans with respect to one of these faces. For instance, with respect to the S_1:S_3:S_4 face, C_1 is cis to this face when oriented trans to

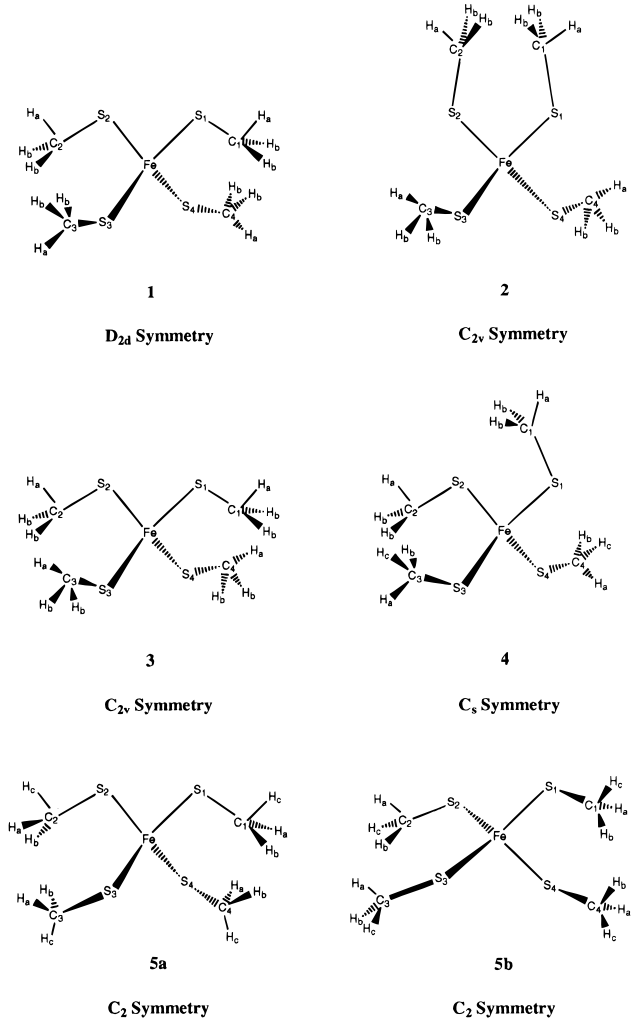

Figure 2. Schematic of the analogue $Fe(SCH_3)_4^-$ in conformations **1**−**5**. Two views of conformation **5** are shown.

S_2 but trans to the face when oriented cis to S_2. Therefore, a given face is spatially hindered most when its carbons are cis to it and is hindered least when its carbons are trans to it.

The different conformations studied here were chosen to mimic the different dihedral angles found in the protein and in various redox site analogues. The conformational degrees of freedom examined include both rotations around the Fe−S bonds and rotations around the S−C bonds (Figure 2). In the most symmetric system studied, **1**, the molecule is of D_{2d} symmetry with all the sulfurs and carbons equivalent to each other by symmetry. Structures **2** and **3** both possess C_{2v} symmetry and **4** is of C_s symmetry while **5** is of C_2 symmetry. The redox site in the protein adopts a conformation similar to **1** or **3**, whereas the Holm−Ibers analog adopts a conformation similar to **5**, where the phenyl rings would be attached to the H_a positions on each of the carbons (compare Figure 1b with **5b** in Figure 2). While all four ligands are cis in both **1** and **3**, two of the methyl groups are cis and two are trans in **2**, whereas in **4** only one ligand is trans. In structure **5** with its C_2 symmetry, the Fe−S dihedrals are not fixed at 0° or 180°. By comparison, in **1** and **3**, C_3 and C_4 are rigorously cis to S_1:S_2:S_3 and S_1:S_2:S_4, respectively, but in **5** the carbons are predominantly trans to these two faces. The plausibility of intercoverting among conformations **1**−**5** was also evaluated since analogues have been synthesized that have ligands which are free to rotate about the aforementioned dihedral angles.[31] Changes resulting from the Fe−S dihedral transitions can be quantified since a 180° rotation around the Fe−S_1 bond in **1** gives conformation

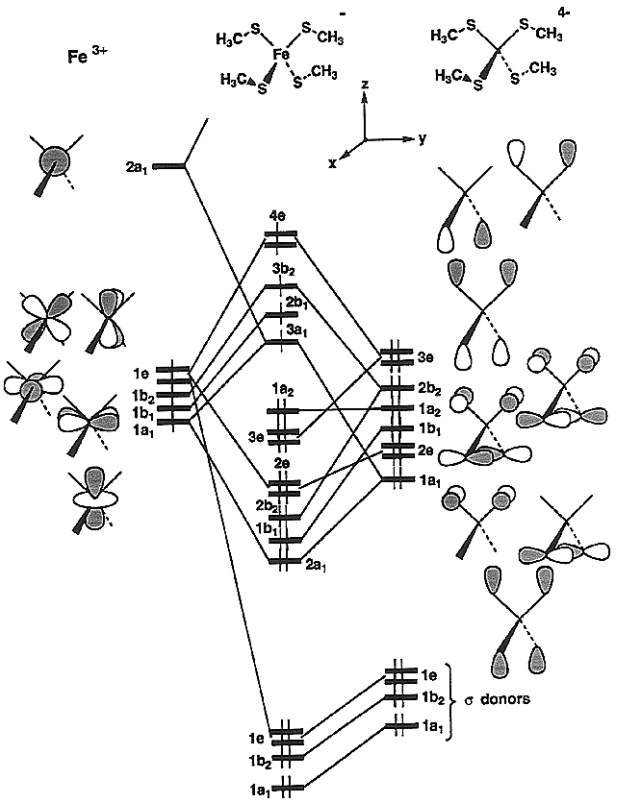

Figure 3. Orbital interaction diagram for $Fe(SCH_3)_4^-$. The molecule is partitioned such that the orbitals of Fe^{3+} are on the left side and orbitals of the four $(SCH_3)^-$ ligands are on the right.

4. Likewise from **3**, 180° rotations around Fe−S_1 and Fe−S_2 yield structure **2**. Finally, the extent to which the S−C bonds play a role can be determined since two of the methyl groups in **3** (those labeled with subscripts 3 and 4) are rotated 180° with respect to their positions in **1**.

The orientation of any given methyl group was idealized, where possible, by restricting one of its hydrogens to lie within the plane containing the methyl carbon (C_β), the sulfur to which the carbon is attached, and the iron. This hydrogen, H_a in Figure 2, may have a dihedral angle of either 0° or 180°. The other two hydrogens of the methyl group, H_b, are equivalent to each other by symmetry in all instances indicated. Where the methyl hydrogens are all inequivalent by symmetry, they are labeled as H_a, H_b, and H_c.

b. Electronic Structure Calculations. The interaction diagram (Figure 3) was constructed from extended Huckel calculations[32] which used a modified Wolfsberg−Helmholtz formula[33] with standard parameters taken from the literature.[34] The following geometric parameters were idealized from the oxidized structure: Fe−S, 2.29 Å; S−C, 1.80 Å; S−Fe−S, 109.5°; Fe−S−C, 105.0°.[35] The methyl groups were also fixed to idealized geometries.

Both the oxidized and reduced states of the model system were examined at the *ab initio* level. The charge of the oxidized form is 1− while that of the reduced form is 2−, making the iron formally Fe(III) in the former and Fe(II) in the latter. Because experiments have shown that the iron is in its high spin state in both cases,[36] unrestricted Hartree−Fock (UHF) calculations were necessary, carried out here using the Gaussian 92[37] and GAMESS[38] electronic structure packages. Electron correlation was included by using second-order perturbation theory (MP2) as implemented in Gaussian 92.

Three different basis sets were implemented at different stages in these calculations. The first of these, BSI, utilizes

an effective core potential (ECP) on the iron and the sulfurs. For both atoms the pseudopotentials remove the 1s, 2s, and 2p electrons from explicit consideration. In addition, the associated bases were used for both iron and sulfur, which were contracted to give a double-zeta basis in the valence region, i.e., (341/311/41) for iron and (21/21) for sulfur.[39,40] The C atoms used the standard 3-21G basis[41] while the methyl hydrogens were represented with the smaller STO-3G basis.[42,43]

The second basis set, BSII, consists of the (14s9p5d) primitive set of Wachters[44] for the iron which was modified in the following way. The last s exponent was changed to 0.298, two p functions were added with exponents of 0.231 and 0.0899, and the d exponents were supplanted with those calculated by Rappe et al.,[45] which were contracted to give (5111111111/41111111/411). The same sulfur basis set used in BSI was employed here but was augmented with a d function ($\zeta = 0.60$). The basis sets on the carbons and methyl hydrogens were unchanged. The third basis set, BSIII, was the same as BSII with an f polarization function ($\zeta = 1.339$) added to the iron atom.[46]

c. Ionization Potentials. Though Koopman's theorem has long been used to estimate the ionization potential (IP) of closed-shell systems,[47] its application to open shells is more dubious. A more direct approach for calculating the IP of a system is to use the so-called ΔSCF method in which separate single-point self-consistent-field (SCF) calculations on the neutral and ionized systems are performed, and the energy of the former is subtracted from that of the latter.[48] This method has given reasonable agreement between experiment and theory for the IPs of iron porphyrins. More importantly, it has been applied to the intermediate and high spin states of these complexes.[49] The ΔSCF approach was used here.

d. Partial Charge Determination. The atom-centered partial charges were obtained for the BSI-optimized geometries and wave functions of models **1**−**4** by both Mulliken population analysis and by fitting charges to the ESP as implemented in GAMESS.[38] To calculate the ESP charges, a set of points must be selected at which the electrostatic potentials are evaluated. Points further than 5.0 Å away from all atoms or within the van der Waals (VDW) radii of any of the atoms in the molecule were discarded. Two different methods for selecting points within this resultant shell were used in this study. In the first, referred to here as the geodesic method,[50] 10 concentric spheres are centered on each atom of the molecule with radii scaled 1.4, 1.45, 1.50, etc., times the atom's VDW radius. Points are evenly distributed on the surfaces of these spheres by placing them at the vertices of icosahedra that are constructed according to a specified level of geodesic tessellation; in this case the total number of points was made comparable to the CHELPG calculations (see below). The set of VDW radii used to determine these geodesic ESP charges are as follows: Fe, 1.8 Å; S, 1.89 Å; C, 1.50 Å; H, 1.20 Å.[51] The second method for arranging the points within the shell is the CHELPG point selection scheme[52] in which the points are spaced 0.5 Å apart, unless otherwise noted, at the vertices of a cubic grid. For the CHELPG calculations, two sets of inner exclusion VDW radii were utilized: the first were proposed by Breneman and Wiberg (referred to here as BW):[52] Fe, 1.8 Å; S, 2.0 Å; C, 1.5 Å; H, 1.45 Å. The second are the Born radii used by Mouesca et al. in their DFT study (referred to here as Born):[19] Fe, 1.5 Å; S, 1.8 Å; C, 1.67 Å; H, 1.32 Å. For both methods, a least-squares fit of the nuclear charges to the potentials at these points is performed, constraining the total charge, Cartesian dipole moment components, and quadrapole moment components to match those determined from the electronic wave function.

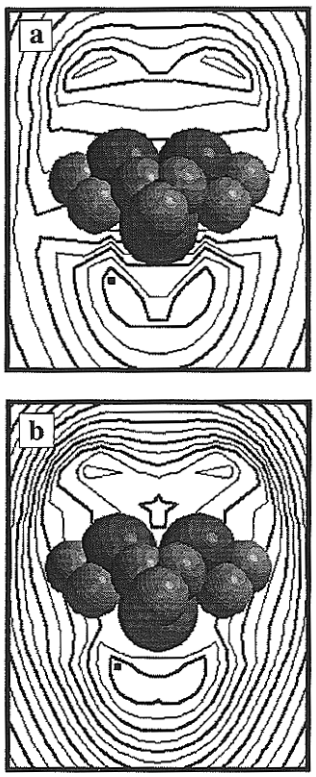

Figure 4. Electrostatic potential contours around the analogue in conformation **1** obtained at the BSIII level on BSII optimized geometries in (a) the oxidized state and (b) the reduced state. All the contours are negative and differ in energy by 0.01 au with the −0.14 contour in (a) and the −0.28 contour in (b) labeled with dark squares. The molecules are represented as fused spheres having the BW radii (see text) centered on the atoms of the BSII optimized geometries. No ESP points within this shell are evaluated. In each figure, the large spheres are sulfurs and the small spheres are hydrogens. The iron is not visible, and the carbons are only slightly visible as dark patches.

3. Results

An overview of the electronic structure of the model complex can be obtained by deriving the valence molecular orbitals (MOs) in an interaction diagram (Figure 3). On the left-hand side of this figure are the unperturbed atomic orbitals of Fe(III) showing the five d electrons. On the right-hand side are the 12 symmetry-adapted linear combinations for the sulfur-based donor orbitals of the methiolates that interact with the iron. The four sulfur σ donor orbitals interact with metal d orbitals to form the four Fe−S bonds labeled $1a_1$, $1b_2$, and 1e in the figure. At intermediate levels in the MO energy manifold are the sulfur π-type donor orbitals that mix with the metal d orbitals. Many of these orbitals are stabilized by the metal d orbitals and transfer electron density from the sulfur to the iron. At highest energy are the metal-based d orbitals, which are antibonding with respect to the sulfur ligand donors. The highest energy of these are the 4e orbitals, which are σ antibonding with respect to the sulfur donor orbitals. The lowest energy member of the five metal-based d orbitals, $3a_1$, is primarily z^2 which has metal s character mixed in to reduce the metal−ligand π antibonding. Upon reduction, the extra electron is added to this MO. These orbital energy levels match those calculated by Noodleman and Case.[18]

The electrostatic potential contours around **1** in the oxidized and reduced states calculated at the BSIII level on the BSII-optimized structures (see below) are shown in Figure 4, a and

TABLE 1: Comparison of Optimized Geometries and Relative Energies of Conformations 1−4 as a Function of Basis Set and Level of Calculation[a]

level	basis set	oxidation state		1	2	3	4
UHF	BSI	oxidized	relative energy	0.0[b]	9.1	1.1	1.0
			$(Fe-S)_{ave}$	2.42	2.42	2.42	2.42
			$(S-C)_{ave}$	1.91	1.90	1.91	1.91
UHF	BSI	reduced	relative energy	0.0[c]	6.6	1.0	0.9
			$(Fe-S)_{ave}$	2.57	2.59	2.57	2.58
			$(S-C)_{ave}$	1.91	1.91	1.91	1.91
MP2	BSI	oxidized	relative energy			0.0[d]	0.7
			$(Fe-S)_{ave}$			2.39	2.39
			$(S-C)_{ave}$			1.94	1.94
MP2	BSI	reduced	relative energy			0.0[e]	1.4
			$(Fe-S)_{ave}$			2.52	2.52
			$(S-C)_{ave}$			1.94	1.94
UHF	BSII	oxidized	relative energy	0.0[f]	9.3	1.2	1.2
			$(Fe-S)_{ave}$	2.37	2.38	2.37	2.37
			$(S-C)_{ave}$	1.84	1.84	1.84	1.84
UHF	BSII	reduced	relative energy	0.0[g]	6.5	1.0	0.8
			$(Fe-S)_{ave}$	2.54	2.56	2.54	2.55
			$(S-C)_{ave}$	1.85	1.85	1.85	1.85
experimental[h]		oxidized	$(Fe-S)_{ave}$		2.29		
			$(S-C)_{ave}$		1.81		
		reduced	$(Fe-S)_{ave}$		2.36		
			$(S-C)_{ave}$		1.81		

[a] Relative energies in kcal/mol and bond lengths in angstroms. [b] Absolute energy is −319.830 11 au. [c] Absolute energy is −319.820 89 au. [d] Absolute energy is −320.485 82 au. [e] Absolute energy is −320.442 36 au. [f] Absolute energy is −1459.770 80 au. [g] Absolute energy is −1459.692 40 au. [h] Experimental geometry for the oxidized bond length from ref 35 and for the reduced bond length from ref 59.

b, respectively. There are zones of high negative potential centered above and below the sulfurs for both states. Referring to the orbital interaction diagram (Figure 3), the pair of spots in the upper half of each of the plots corresponds to the density associated with the MOs labeled 3e and $2b_2$ while the dumbbell in the lower half of each of the plots corresponds to the density associated with the pair of ligand fragment orbitals labeled 2e and $1b_1$. These orbitals are doubly occupied and thus harbor substantial electron density in the lone pair regions shown. These features persist in both the oxidized and reduced states though the potentials are much steeper for the reduced 2− complex (Figure 4b) when compared to the oxidized 1− complex (Figure 4a). The effects of the orientation of these electrostatic potentials in the different conformations and the depth of the contours on the magnitudes of the atom-centered partial charges are examined below.

a. Geometries. The dependence of the optimized geometries on the basis set and electron correlation was studied (Table 1). Conformations **1**−**4** were optimized at the UHF level using BSI and BSII, and conformations **3** and **4** were optimized at the MP2 level using BSI. The UHF structures from BSI, which used an ECP on Fe, exhibited Fe−S bond lengths that were too long by 0.13 Å for the oxidized and 0.21 Å for the reduced compared with experiment. The MP2 optimizations consistently reduced the Fe−S bond lengths from the UHF values, which brought them closer to the experimental measurements, although they are still too long by 0.1 Å for the oxidized state and 0.16 Å for the reduced state. In contrast, the average S−C bond lengths for either redox state increased from 1.91 Å at the UHF level to 1.94 Å for the MP2 structures whereas the experimental number is 1.81 Å. On going from BSI to BSII, in which the iron now has an explicit core representation and the basis set on the sulfur was augmented with a polarization function (see methods), at the UHF level, the most prominent differences are that, at the higher level, the Fe−S bonds are 0.05 Å shorter for the oxidized and 0.03 Å shorter for the reduced and the S−C bonds are 0.07 Å shorter for the oxidized and 0.06 Å shorter for the reduced. Thus, BSII shows best agreement with experimental bond lengths.

More detailed analysis of the optimized geometries was made for the BSII structures (Table 2). These structures show that the Fe−S bond lengths are uniform among all the conformations, with the exception of structure **2**. This structure has a pair of longer Fe−S bonds ($Fe-S_1$ and $Fe-S_2$) because of steric crowding between the methiolate ligands, also indicated by the S_1-Fe-S_2 angles that widen to 116.2° for the oxidized and 115.1° for reduced states, respectively. For the rest of the structures, the average S−Fe−S angles are very close to the expected tetrahedral value of 109.5°. The average Fe−S−C angles are all about 100°−101° for all structures, which is smaller than the 109.3° angle seen in $[Ti(\eta^5\text{-}C_2H_5)_2(SC_2H_5)_2]$[53] or the 110° angle observed for various mercaptophenyl ligands[54,55] but is substantially larger than the 92.1° angle reported for H_2S.[56] In geometry **2** with the steric crowding, the Fe−S−C angles associated with ligands 1 and 2 are more obtuse: 112.9° for the oxidized structure and 110.9° for the reduced.

b. Atomic Spin Populations. An analysis of the atomic spin populations has been made, along with the spin contamination, S^2, which gives a measure of the quality of the UHF wave function (Table 3). The atomic spin population on the iron atoms closely approach the ideal value of +5 for the oxidized structures, while the populations for the reduced irons are even closer to the ideal +4. As expected, most of the unpaired density in the complex is concentrated at the metal; however, the ligands bear a larger percentage of the spin population in the oxidized state versus the reduced state simply because there is more total spin concentrated on a smaller molecular structural framework. For all conformations, the atomic spin population on the iron decreases as the complex is reduced from Fe(III) to Fe(II), since adding the sixth electron to the Fe(III) cancels the spin density from one of the five unpaired electrons originally present.

The discrepancy between the actual and ideal atomic spin population on Fe gives a measure of the electron delocalization present. The reduced structures are close to the localized valence bond (VB) limit since nearly all of the spin is localized on the iron; i.e., the covalent components in the bonds are small for this electronic state. The ratio of the actual to the ideal spin population at the iron is one measure of this metal−ligand covalency. The oxidized structures yield a range of 92.3−92.5%

TABLE 2: Relative Energies and Geometries for Conformations 1−5 Optimized Using BSII at the UHF Level[a]

oxidation state		1	2	3	4	5
oxidized	relative energy	0.0[b]	9.3	1.2	1.2	2.6
	$Fe-S_1$ ($Fe-S_2$)	2.37	2.39	2.37	2.38 (2.38)	2.37
	$Fe-S_{3,4}$	2.37	2.36	2.37	2.37	2.38
	S_1-Fe-S_2	104.3	116.2	103.5	104.9	105.2
	$S_{1,2}-Fe-S_{3,4}$[d]	112.1	109.6	112.6	112.9 (111.4)	106.2 (116.2)
	S_3-Fe-S_4	104.3	101.0	103.2	103.6	107.2
	$Fe-S_1-C_1$ ($Fe-S_2-C_2$)	100.4	112.9	100.4	104.5 (100.5)	102.2
	$Fe-S_3-C_3$	100.4	102.5	102.1	100.8	105.3
	$(S-Fe-S)_{ave}$	109.5	109.3	109.5	109.5	109.5
reduced	relative energy	0.0[c]	6.5	1.0	0.8	2.0
	$Fe-S_1$ ($Fe-S_2$)	2.54	2.59	2.54	2.56 (2.55)	2.54
	$Fe-S_{3,4}$	2.54	2.53	2.54	2.54	2.56
	S_1-Fe-S_2	107.9	115.1	107.6	106.5	108.0
	$S_{1,2}-Fe-S_{3,4}$[d]	110.3	108.6	110.7	111.9 (109.3)	106.7 (114.9)
	S_3-Fe-S_4	107.9	106.8	106.6	108.0	105.9
	$Fe-S_1-C_1$ ($Fe-S_2-C_2$)	100.2	110.9	99.9	101.8 (99.4)	101.9
	$Fe-S_3-C_3$	100.2	102.6	102.4	100.2	102.0
	$(S-Fe-S)_{ave}$	109.5	109.4	109.5	109.5	109.5

[a] Relative energies in kcal/mol, bond lengths in angstroms, and bond angles in degrees. [b] Absolute energy is −1459.770 80 au. [c] Absolute energy is −1459.692 40 au. [d] For conformation **4**, values are for $S_1-Fe-S_{3,4}$ ($S_2-Fe-S_{3,4}$) and for conformation **5**, values are for $S_{1,2}-Fe-S_{3,4}$ ($S_{1,4}-Fe-S_{2,3}$).

TABLE 3: Basis Set Dependence of Atomic Spin Populations and S^2 Values for Conformations 1−4

basis set	oxidation state	atom	1	2	3	4
BSI	oxidized	Fe	4.345	4.334	4.338	4.341
		$(S)_{ave}$	0.163	0.164	0.165	0.165
		$(H_3C)_{ave}$	0.000	0.002	0.001	−0.001
		S^2	8.773	8.773	8.773	8.773
BSI	reduced	Fe	3.970	3.972	3.966	3.971
		$(S)_{ave}$	0.009	0.008	0.010	0.009
		$(H_3C)_{ave}$	−0.003	−0.001	−0.002	−0.003
		S^2	6.010	6.009	6.010	6.010
BSII	oxidized	Fe	4.625	4.617	4.617	4.623
		$(S)_{ave}$	0.088	0.090	0.090	0.090
		$(H_3C)_{ave}$	0.005	0.006	0.006	0.005
		S^2	8.771	8.771	8.770	8.771
BSII	reduced	Fe	3.965	3.966	3.961	3.967
		$(S)_{ave}$	0.010	0.009	0.011	0.009
		$(H_3C)_{ave}$	−0.002	−0.001	−0.002	−0.002
		S^2	6.014	6.014	6.014	6.014

ionicity of the Fe−S bond, whereas the reduced structures exhibit a range of 99.0−99.2% ionicity or only 0.8−1.0% covalency in the Fe−S bond.

c. Energies. The dependence of the relative energies of conformations **1**−**4** on the level of calculation and the basis set was studied first (Table 1). The relative energies obtained using BSI are within 0.2 kcal/mol to those obtained using BSII. Furthermore, the relative energies exhibit the same pattern among the conformations in both the oxidized and reduced states. **1** is the lowest energy conformation, and **2** is the highest; **1**, **3**, and **4** are all within 1.1 kcal/mol of each other. The MP2 relative energies give results similar to those found at the UHF level; i.e., for the two structures examined the relative energy differences are minimal. The conformational variation in the relative energies was studied for all five conformations using the highest level BSII results (Table 2). These are discussed in terms of steric interactions in the Discussion section.

Next, IPs were calculated by the ΔSCF method using the absolute single point energies for conformation **1** calculated at the BSII level. For the reduced geometry, the ionization from the reduced (red) to the oxidized state (oxd*) gives an IP of −1.56 eV, while for the oxidized geometry the ionization from the reduced state (red*) to the oxidized (oxd) gives an IP of −2.57 eV (Figure 5). The average of these two numbers, −2.06 eV, represents the IP for the oxidation of a hypothetical structure halfway between the oxidized and reduced geometries. To check the basis set dependence, these calculations were repeated with the same geometries using BSIII. The IPs were only slightly less: −1.50 eV for the reduced geometry and −2.52 eV for the oxidized geometry for an average of −2.01 eV; therefore, BSII was deemed sufficient for the IP calculations. For the BSII energies, the two IPs were related using the construct of geometrical relaxation, which must be included when calculating the total energy change upon changing redox state, ΔE_{redox}. ΔE_{redox} is simply the difference in energy of oxd and red, and it may be termed an adiabatic ionization potential. For the oxidized state, oxd* is 0.57 eV higher than oxd, where for the reduced state, red* is +0.44 eV higher in energy than red. The former is extra stabilization energy gained after oxidation, while the latter is the energetic cost to ready the structure for the oxidation process. Therefore, for the ionization of red to oxd, the geometrical relaxation adds −0.57 eV to −1.56 eV or subtracts 0.44 eV from −2.57 eV to give −2.13 eV, which is fortuitously close to the −2.06 average of the ΔSCF IPs.

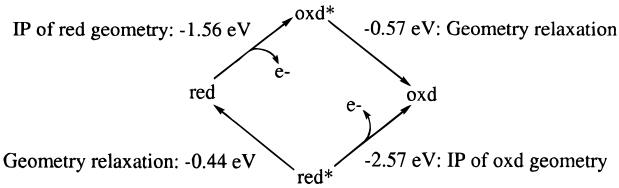

Figure 5. Schematic showing the ionization energies of conformation **1** for both the BSII optimized reduced geometry (reduced state, red; oxidized state, oxd*) and the BSII optimized oxidized geometry (reduced state, red*; oxidized state, oxd). The absolute energies used for these calculations are as follows: Oxd, −1459.770 80 au; Oxd*, −1459.749 82 au; Red*, −1459.676 46 au; Red, −1459.692 39 au.

The degree to which conformation plays a role in the electron-transfer properties of the protein can be ascertained from the ΔE_{redox} energies of models **1**−**5**. Using BSII energies, ΔE_{redox} values are as follows: **1**, −2.13 eV; **2**, −2.01 eV; **3**, −2.12 eV; **4**, −2.12 eV; **5**, −2.10 eV. The BSIII results on **1** suggest that these should be reduced by 0.05 eV. Nonetheless, these ΔE_{redox} values are very similar with the exception of that for **2**.

d. Partial Charges. The Mulliken charges were calculated for **1**−**4** at the BSI level (Table 4). There is little variation in the partial charge distribution as a function of the dihedral rotations as seen by the homogeneity in the charge on iron and the average sulfur and methyl charges. However, in both states,

TABLE 4: Mulliken, Geodesic and CHELPG Charges for Conformations 1−4 Calculated at the UHF Level Using BSI

charge	oxidation state	atom	**1**	**2**	**3**	**4**
Mulliken	oxidized	Fe	0.386	0.397	0.380	0.392
		$(S)_{ave}$	−0.172	−0.153	−0.170	−0.173
		$(H_3C)_{ave}$	−0.175	−0.196	−0.175	−0.175
Mulliken	reduced	Fe	0.495	0.506	0.494	0.500
		$(S)_{ave}$	−0.365	−0.350	−0.364	−0.367
		$(H_3C)_{ave}$	−0.259	−0.276	−0.260	−0.258
geodesic	oxidized	Fe	1.243	1.065	1.522	1.216
		$(S)_{ave}$	−0.665	−0.559	−0.720	−0.656
		$(H_3C)_{ave}$	0.104	0.043	0.090	0.102
geodesic	reduced	Fe	1.333	1.066	1.584	1.210
		$(S)_{ave}$	−0.874	−0.722	−0.922	−0.838
		$(H_3C)_{ave}$	0.041	−0.044	0.026	0.036
CHELPG	oxidized	Fe	1.511	1.371	1.616	1.418
		$(S)_{ave}$	−0.775	−0.730	−0.765	−0.759
		$(H_3C)_{ave}$	0.147	0.137	0.111	0.154
CHELPG	reduced	Fe	1.427	1.211	1.506	1.275
		$(S)_{ave}$	−0.936	−0.855	−0.931	−0.900
		$(H_3C)_{ave}$	0.079	0.052	0.055	0.081

the iron of **2** has more positive charge, and the average sulfurs of **2** have less negative charge versus the other conformations.[57] For all of the conformations examined, the Mulliken charge on the iron atom becomes surprisingly more positive upon reduction, which is addressed below.

Both the geodesic and CHELPG charges of **1**−**4** calculated at the BSI level (Table 4) show some of the same trends as the Mulliken charges. For instance, regardless of oxidation state, the average ESP sulfur charge is smallest for **2**, whereas opposite from the Mulliken charges, the iron is smallest for **2.** Also, the ESP charges exhibit a much stronger conformational dependence than the Mulliken charges, although the dependence for the CHELPG charges is weaker than the geodesic. For instance, the charge on iron for CHELPG spans a range of 0.245 *e* for the oxidized and 0.295 *e* for the reduced systems whereas for geodesic it spans a range of 0.457 *e* for the oxidized and 0.518 *e* for the reduced systems. Finally, CHELPG charges show a decrease in positive charge on the iron atom upon reduction for all of the conformations examined, whereas, like the Mulliken charges, the geodesic charges exhibit a small increase in all cases except conformation **4**.

The increase in positive charge on the iron upon reduction for the Mulliken and geodesic methods, and the corresponding decrease for the CHELPG charge (Table 4), was investigated more fully at the BSIII level for conformation **1** (Table 5). When charges were calculated from Mulliken populations for the oxidized and reduced states while keeping the geometry of a given state, there is a decrease in positive charge on the iron upon reduction with either geometry, which follows the chemically intuitive trend. Thus, the increase in positive charge upon reduction noted in Table 4 is due to the change in bond lengths, primarily, and not to a decrease in electron density on the iron. However, now both of the ESP charges, which were calculated with high point densities (CHELPG grid spacing was 0.25 Å), show the counterintuitive trend.

Because the CHELPG method is widely used to calculate partial charges for molecular dynamics simulations, the fitting parameters were examined in detail using BSIII. When the point density around the molecule was increased by reducing the grid spacing between points from 0.50 to 0.25 Å, increasing the number of points by nearly an order of magnitude (Table 6), very little difference was observed in the partial charges. This justifies the use of the course grid (0.5 Å) and verifies the previously reported finding that the charges stabilize after a certain threshold of points/atom is reached.[58] The effect of using

TABLE 5: Comparison of the Oxidized and Reduced Mulliken, Geodesic, and CHELPG Charges for Conformation 1; Wave Functions Calculated at the UHF Level Using BSIII for BSII Optimized Geometries

charge	oxidation state	atom	oxidized geometry	reduced geometry
Mulliken	oxidized	Fe	0.727	0.754
		$(S)_{ave}$	−0.275	−0.292
		$(H_3C)_{ave}$	−0.157	−0.146
Mulliken	reduced	Fe	0.707	0.740
		$(S)_{ave}$	−0.445	−0.466
		$(H_3C)_{ave}$	−0.232	−0.220
geodesic	oxidized	Fe	1.071	1.094
		$(S)_{ave}$	−0.583	−0.590
		$(H_3C)_{ave}$	0.064	0.067
geodesic	reduced	Fe	1.336	1.248
		$(S)_{ave}$	−0.839	−0.826
		$(H_3C)_{ave}$	0.005	0.013
CHELPG	oxidized	Fe	1.328	1.259
		$(S)_{ave}$	−0.678	−0.658
		$(H_3C)_{ave}$	0.095	0.093
CHELPG	reduced	Fe	1.448	1.298
		$(S)_{ave}$	−0.898	−0.867
		$(H_3C)_{ave}$	0.036	0.043

BW versus Born inner exclusion radii in calculating the ESP charges for a common wave function were also compared (Table 6). The shell of points is thicker for the Born systems since the VDW radii for all BW atoms, except carbon, are smaller than the Born radii. Only small differences are apparent when comparing these BW charges with the Born charges. However, the errors in the ESP charges determined using the Born models are higher than the corresponding BW values by 25−32%.

A comparison of the ESP charges on the optimized versus experimental geometries is also provided (Table 6). For the experimental geometries, all the bond angles and dihedral angles obtained from the optimized structures were held fixed except that the Fe−S bonds were reduced to the experimental values of 2.29[35] and 2.36 Å[59] for the oxidized and reduced states, respectively (Figure 6). These bond length reductions result in an increase in the polarization of the Fe−S bonds; the average charge on the iron is about 0.23 *e* more positive, and each of the sulfurs is 0.06 *e* more negative. Predictably, there is a modest increase in error, both root mean square and relative, which accompanies the contraction of this shell of points toward the molecule.

4. Discussion

a. Basis Sets and Level of Calculation. For the models used in this study, the higher level calculations predictably give more accurate optimized geometries. Less expected are the rigorously proportionate changes in geometrical parameters among conformations **1**−**4** as the number of basis functions increase. Moreover, the relative energies between conformations obtained at the different basis set levels are remarkably similar, and the MP2 relative energies change little from the uncorrelated results. It is interesting to note that while the Fe−S bond lengths at the UHF level using BSII are similar to those at the MP2 level using BSI, the S−C bond lengths are better for BSII without the MP2 calculation. An MP2 calculation using BSII, which would not be computationally feasible, would include excited state configurations in which the core basis functions on the iron were vacated; thus, we would expect a more dramatic move toward an accurate optimized geometry. Nevertheless, results in this study suggest that including higher order corrections would not cause a large change in the relative stability of one conformation versus that of another. The energy difference between the oxidized and the reduced state, ΔE_{redox},

TABLE 6: Comparison of CHELPG Partial Charges Fit Using Different Grid Sizes, Exclusion Radii and Geometries for Conformation 1; Wave Function Calculated at the UHF Level Using BSIII for Geometries Optimized at the BSII Level

		BW radii[a]			Born radii[b]	
oxidation state	atoms	optimized[c]	optimized[c]	expt.[d]	optimized[c]	expt.[d]
oxidized	Fe	1.328	1.335	1.492	1.387	1.593
	S	−0.678	−0.672	−0.735	−0.700	−0.771
	C	0.088	0.042	−0.019	0.157	0.070
	H_a	0.057	0.070	0.099	0.044	0.073
	H_b	−0.025	−0.012	0.006	−0.049	−0.010
	(H_3C)	0.095	0.088	0.092	0.103	0.123
	grid spacing	0.25	0.50	0.50	0.50	0.50
	points	111912	14008	13912	14372	14208
	rms[e]	1.54	1.55	1.97	2.04	2.50
	relative[f]	2.74	2.77	3.48	3.58	4.36
reduced	Fe	1.298	1.300	1.579	1.293	1.564
	S	−0.867	−0.877	−0.936	−0.875	−0.948
	C	0.042	0.103	−0.182	0.096	−0.065
	H_a	0.033	0.017	0.108	0.016	0.072
	H_b	−0.016	−0.034	0.057	−0.030	0.025
	(H_3C)	0.043	0.052	0.040	0.052	0.057
	grid spacing	0.25	0.50	0.50	0.50	0.50
	points	115390	14436	13976	14830	14338
	rms[e]	1.82	1.79	2.14	2.37	2.78
	relative[f]	1.68	1.62	1.91	2.10	2.44

[a] Breneman and Wiberg radii (Å): Fe, 1.8; S, 2.0; C, 1.5; H, 1.45. [b] Born radii (Å): Fe, 1.5; S, 1.8; C, 1.67; H, 1.32. [c] Optimized geometries are those listed in Table 2. [d] Experimental geometries maintained all bond lengths and angles in Table 2 except for the Fe−S bonds which were contracted to match experimental values; oxidized, 2.29 Å; reduced, 2.36 Å. The relative energies of these structures with respect to the optimized geometries were 30.9 and 36.4 kcal/mol for the oxidized and reduced, respectively. [e] Root-mean-square deviation in kcal/mol. [f] Relative root-mean-square deviation in %.

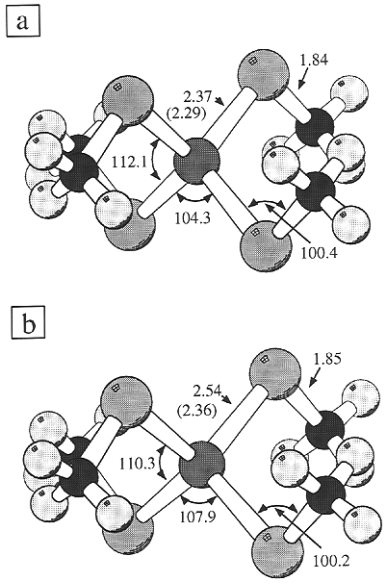

Figure 6. Ball-and-stick figures of the analogue in conformation **1** showing select geometrical parameters from the UHF optimizations using BSII for (a) the oxidized state and (b) the reduced state (bond lengths in angstroms and bond angles in degrees). Also shown in parentheses are the experimental Fe−S bond lengths. The shading from light to dark indicates H, S, Fe, and C.

for the rubredoxin like conformation, −2.13 eV, is lower than the −1.79 eV value reported by Mouesca et al.[19] and −1.67 eV from Goddard III et al.[14] The accuracy of this value remains to be proven. In terms of absolute accuracy of the geometries, the errors in the Fe−S bond lengths are significant, but predictable, as is frequently the case with UHF calculations.[60,61]

In terms of spin contamination, for every conformation, regardless of basis set, the actual S^2 values are very close to the ideal values of 8.75 and 6.00 for high spin Fe(III) and Fe(II), respectively. This signifies very little spin contamination in the UHF wave functions. In addition, the S^2 values of 8.77 for the d^5 systems are the same as that determined for the high spin Fe(III) hydroperoxide calculated at a similar level.[46] The atomic spin populations do show some basis set dependence in the oxidized state where there is more spin on the iron in the BSII wave functions versus the BSI wave functions. In contrast, the reduced state exhibits little difference in the spin density at the iron between BSI and BSII. Like the geometries, the relative differences between the atomic spin populations are well reproduced when the ECP is on iron, but in absolute terms, the ECP does introduce some error into the results by excluding too much spin on the iron atom for the high spin oxidized state. The atomic spin population on the iron calculated using BSII, 4.62, also compares favorably to the 4.82 calculated for the Fe(III) hydroperoxide.[46]

In summary, BSI and BSII UHF calculations give remarkably similar results in terms of relative energies, geometric changes between conformations, and absolute atomic spin populations and S^2 values. These results clearly illustrate the efficacy of the ECP in reproducing the electronic properties of the all-electron basis set on iron. The major difference between the two levels is in the bond lengths. While the iron is apparently well depicted electronically at all levels tested, the sulfur is not at the BSI level. The role of the polarization function for properly describing the bonding in second-row elements is well-known.[62−64] While this role is critical for some applications, it does not seem to be the case for examining the conformational stability for the present model. Therefore, relative differences between electronic properties among conformations can be discerned using BSI, but accuracy in absolute quantities such as partial charges and IPs warrants use of the larger basis sets.

b. Partial Charges. The characterization of partial charges via quantum mechanical procedures is often ambiguous due to the lack of readily available experimental quantities for comparison. Nonetheless, inferences regarding a particular method for calculating accurate charges can be drawn based on chemical intuition. Mulliken's method is not optimal for partial charge determinations, especially because of problems with basis set dependence in this study and in previous cases.[65,66] Though the geometries from BSI are only slightly different from the BSII structures (Table 1), the Mulliken charge on the Fe for **1**

calculated with BSIII (Tables 5) is nearly twice as large as that calculated with BSI (Table 4). Serious deficiencies have also been reported for similar metals; for instance, in DFT studies of Os(II) hydride complexes, a negative Mulliken charge on the osmium was reported, whereas the more accurate atoms-in-molecules approach (AIM) gave the expected positive charge on the Os atom.[67] In addition, the Mulliken charges do not reproduce the higher moments of the electron density since the magnitudes of the charges are much less polar.

However, the Mulliken charges do provide information since they are directly related to the electron density whereas ESP fitting methods, which are fits to the electrostatic potential due to the electron density, are indirect indictors. Thus, Mulliken charges are less subject than ESP charges to problems such as those associated with buried atoms. Consider, for instance, the increase upon reduction in the Mulliken charge on the unexposed Fe (see Figure 4) in the present study (Table 4). The addition of the extra electron to the metal-based d orbital could cause so much electronic relaxation in the ligand based orbitals that a decrease in the density at the iron occurs. However, when the molecule was held to a fixed geometry, the charge on iron decreased upon reduction (Table 5), the chemically intuitive trend. Since the Mulliken population analysis partitions half the overlap probability density to each of the atomic orbitals in the Fe−S bonds, this result suggests that the sulfurs and iron retain at least all of their originally held electron density upon reduction. Since the Fe−S bond actually increases in length upon reduction, the overlap between the metal and ligand orbitals will decrease. Apparently, this results in a reduction in the overlap population and less metal−ligand charge transfer and an increase on the charge on the iron. This is further exhibited by the increase in Fe charge for a given oxidation state when going from the oxidized to the reduced geometries (Table 5). Moreover, the Mulliken charges are relatively invariant with respect to conformation, as would seem intuitive since the conformations differ by the placement of the relatively distant methyl groups. Since these are two chemically intuitive points; i.e., reduction of charge on the Fe upon reduction of the molecule and conformational invariance of these charges, both seem to be reasonable criteria by which to judge the different ESP methods for generating charges.

ESP charges were developed, in part, to correct problems associated with basis set dependency. The basis set dependence is much smaller for the ESP charges versus the Mulliken, as can be seen by comparing the ESP charges for **1** obtained using BSI (Table 4) to those obtained using BSIII (Table 6), though the geometries are slightly different (Table 1). While point density and the size of the excluded volume around the molecule had only marginal effects on the ESP charges, more modest changes in the molecular geometries did have a moderate impact. A 3−9% reduction in the Fe−S bond length results in a 10% increase in negative charge for each sulfur and thus a large change in the charge on the iron. Also, the different conformations exhibited a range of charges on the sulfurs and the iron. This confirms the previously made observation that charges calculated for buried atoms are more subject to fluctuation.[68] In contrast, the charges on the methyl groups are more impervious to the geometrical perturbation, due to their uniform exposure for all geometries (Table 6). However, for a given geometry and wave function, differences in points selected for the ESP fits can dramatically affect the partial charges (Table 5). Though the number of points was roughly equivalent for each, the geodesic and CHELPG charges gave qualitatively different results regarding the redox couple and conformational dependence. Because CHELPG gives the chemically intuitive result that the charges are less conformationally dependent and the charge on iron decreases upon reduction after relaxation, we recommend these charges for use in molecular dynamics simulations (first column of Table 6).

When comparing the results of this study to the previous DFT results,[19] which used CHELPG and the Born exclusion radii to fit the ESP charges, there are similarities and differences in the partial charge distribution.[69] For instance, for both the conventional *ab initio* and the DFT results, the sulfurs accept most of the incoming electron density upon reduction. Although chemical intuition predicts that the iron will accept some of this excess density, only the CHELPG charges calculated in this study support this assumption whereas the most recent DFT does not. However, earlier Xα scattered wave calculations[18] also support this assumption. Nonetheless, the relative insensitivity of the ESP to fitting buried charges makes the charge on iron a less important criteria. Moreover, the CHELPG bonds in this study are much more polarized when compared to the other methods, including DFT/CHELPG. This polarity increases even more when experimental geometries and Born exclusion radii, like those in the DFT study, are used (Table 6). Clearly, the higher polarity in the present study is due to a different electronic structure than that calculated with the DFT method. Our results are similar to those reported from *ab initio* SCF wave functions of [2Fe] sites where the Fe(III) and Fe(II) were assigned charges of +1.47 and +1.34, respectively.[70] Moreover, a recent study comparing density functional and conventional *ab initio* results for a series of Os(II) complexes also showed that the partial charge on the Os was highly dependent on the computational method, with the DFT results giving less polar bonds than the conventional *ab initio* results though the authors refrain from recommending one method over another.[67] Other work on small molecules generally suggests LDA, especially with nonlocal corrections, will do better than HF for predicting experimental dipole moments,[27] although comparisons with organometallics have not been verified experimentally. On the other hand, suggestions have been made that more polar distributions than those from gas phase are needed to adequately describe the moments in condensed phases.[71]

c. Conformation. For [1Fe], experimentally and in our model system, sterics dictate certain aspects of the ligand configurations of the five conformations studied. Relative to conformation **1**, conformation **3** is slightly less energetically favored due to cis orientation of the $Fe-S_{3,4}-C_{3,4}-H_a$ dihedral. Apparently, in **1**, steric interactions between the H_bs of C_2 with those of C_3 and the H_bs of C_1 with those of C_4 are less important. Also relative to conformation **1**, conformation **4** is slightly less energetically favored due to the rotation about the $Fe-S_1$ bond. Since both **3** and **4** can be considered as transition states for dihedral rotations, it appears that rotations about the S−C and Fe−S bonds are relatively free. On the other hand, structure **2** has a higher relative energy than the rest mainly due to the steric interaction between the two trans methiolate ligands, which cannot be relaxed completely due to the symmetry imposed on the model. This relative energy represent a sizable barrier for two simultaneous dihedral transitions at ambient temperatures. Finally, conformation **5,** which has trans-like $S_1-Fe-S_3-C_3$ and $S_1-Fe-S_4-C_4$ bonds, rather than cis bonds as in conformation **1**, has more steric interaction between C_2 and C_3 and C_1 and C_4 than in conformation **1**. Although this conformation is at a minimum with respect to these dihedrals, this structure is higher in energy than either **3** or **4**. Thus, although conformation **5** would be less favored if there is free rotation

about the Fe−S bond, in the Holm−Ibers analogue, this conformation is constrained by the xylyl rings.

Steric affects will slightly alter the metal−ligand configuration, which ultimately will affect the electronic structure at the metal. The following conformational preferences of bis-thiolate ligands for d^0 and d^2 systems have been determined: the endo configuration (ligands 3 and 4 in structure **5**) is preferred for the d^0 system while the exo configuration (ligands 1 and 2 in structure **5**) is preferred for the d^2 system. The π interactions between the sulfur donors and the metal are different for the two configurations, hence the enhanced stability of one orientation over another depending on the electron count.[53,72]

Similar considerations are valid for the d^5 and d^6 electron counts here. For a given ligand configuration, the orbital energies will dictate the relative energies of the oxidized and reduced structures. Like the d^0 and d^2 systems, the ligand configuration here is important in the relative energy determinations. The Fe−S bonds expand upon reduction of the model complex regardless of computational level or basis set size. This change in geometry can be rationalized by referring back to MO $3a_1$ from Figure 3. The added electron occupies this d-centered orbital, which is primarily Fe−S antibonding in character; therefore, to reduce the antibonding, the bond lengths expand. The magnitude of this change depends on the level of calculation.

When comparing one conformation to another, small changes in the S−Fe−S angle, for example, can also alter the energy difference between the oxidized and reduced states differently, due to the orbital structure of $3a_1$. Since the difference in energy between the oxidized and reduced states is simply the ΔE_{redox}, these influences would result in different ΔE_{redox} values for different conformations and thus different redox potentials. Such appears to be the case, to a minor degree, in the models examined in this study. The two structures with the endo ligands (**2** and **5**) have smaller negative ΔE_{redox} values, −2.01 and −2.10 eV, respectively, than the other three structures which have ΔE_{redox} values of −2.12 to −2.13 eV. Though the magnitude of this difference is small, it illustrates how the redox potential of an analogue or a protein is modulated by differences in dihedral conformations.

Overall, besides the improbable structure **2**, the results indicate little dependence of the electronic properties of the [1Fe] site with respect to the conformations examined, and furthermore, reasonable pathways for interconverting from one to another are also unlikely to perturb the electronic structure significantly. Most important, this suggests that, at most, about 0.03 V of the 0.8 V difference in redox potential between the Holm−Ibers analogue and the protein rubredoxin can be attributed directly to a change in ΔE_{redox}. Of course, differences in the structure can lead to different environments which could then influence ΔE_{redox}. Moreover, although the magnitudes of ΔE_{redox} may be in some question given difficulties in predicting ionization potentials using HF methods relative to DFT, the relative conformational energetics are likely to be accurate given the successes of HF for conformational energetics.[27] In addition, independence of the relative energetics on the basis set or the inclusion of correlation further supports the conformational energetics.

5. Conclusions

High-level *ab initio* calculations have been performed on the [1Fe] site. The largest basis set at the UHF level gave reasonable geometries, which were actually better than those MP2 calculations which used an ECP on Fe. Although the Hay/Wadt pseudopotentials on the iron reproduces the relative energies for all conformations remarkably well when compared to those determined with the full core basis set, significant differences in the ECP partial charge indicate it is not sufficient for determining these properties.

Of the three methods used to assign the atom-centered partial charges, the CHELPG ESP procedure gave the most reasonable results. When compared to earlier DFT results, the wave functions calculated here predict more polar Fe−S bonds and, unlike DFT, a reduction of the positive ESP charge on the iron after the complex is reduced and geometry relaxation is accounted for. Moreover, the homogeneity of the partial charges for the conformations examined, particularly by Mulliken population analysis, suggest that one set of partial charges will suffice for simulations of molecules containing the [1Fe] site. Based on this, a set of CHELPG charges at the UHF level with BSIII are proposed.

Finally, the conformations studied are very close in relative energies, ΔE_{redox}, geometries, atomic spin populations, and partial charges regardless of basis set or level of calculation, except for one conformation, which has steric repulsion between the methyl groups. Overall, the energetics of interaction of the [1Fe] site with the environment may be considered to depend only on changes in the conformation and not in the partial charge distribution. Moreover, based on the calculated ΔE_{redox}, only about 30 mV of the 800 mV difference in redox potential between rubredoxin and the Holm−Ibers analogue can be attributed to a change in the electronic structure of the [1Fe] site.

Acknowledgment. This research was supported by a grant from the National Institutes of Health (GM45303) and by a grant from the Pittsburgh Center (MCB950005P), sponsored by the National Science Foundation, for time on their CRAY C90 and DEC Alpha Supercluster. We also thank the Maui High Performance Computing Center for the generous allocation of computer time on their SP2.

References and Notes

(1) Cammack, R. *Adv. Inorg. Chem.* **1992**, *38*, 281.
(2) Tsibris, J. C. M.; Woody, R. W. *Coord. Chem. Rev.* **1970**, *5*, 417.
(3) Holm, R. H.; Ibers, J. A. Synthetic Analogues of the Active Sites of Iron-Sulfur Proteins. In *Iron-Sulfur Proteins*; Lovenberg, W., Ed.; Academic Press: New York, 1977; Vol. 3, p 205.
(4) Holm, R. H. *Adv. Inorg. Chem.* **1992**, *38*, 1.
(5) Yang, Y.; Beck, B. W.; Shenoy, V. S.; Ichiye, T. *J. Am. Chem. Soc.* **1993**, *115*, 7439.
(6) Kassner, R. J. *Proc. Natl. Acad. Sci. U.S.A.* **1972**, *69*, 2263.
(7) Shen, B.; Jollie, D. R.; Stout, C. D.; Diller, T. C.; Armstrong, F. A.; Gorst, C. M.; La Mar, G. N.; Stephens, P. J.; Burgess, B. K. *J. Biol. Chem.* **1994**, *269*, 8564.
(8) Gleason, F. K. *Protein Sci.* **1992**, *1*, 609.
(9) Zeng, Q.; Smith, E. T.; Kurtz, D. M.; Scott, R. A. *Inorg. Chim. Acta* **1996**, *242*, 245.
(10) Schejter, A.; Eaton, W. A. *Biochemistry* **1984**, *23*, 1081.
(11) Meyer, T. E.; Prezysiecki, J. A.; Watkins, J. A.; Bhattacharyya, A.; Simondsen, R. P.; Cusanovich, M. A.; Tollin, G. *Proc. Natl. Acad. Sci. U.S.A.* **1983**, *80*, 6740.
(12) Loew, G. H.; Chadwick, M.; Steinberg, D. A. *Theor. Chim. Acta* **1974**, *33*, 125.
(13) Bair, R. A.; Goddard III, W. A. *J. Am. Chem. Soc.* **1977**, *99*, 3505.
(14) Bair, R. A.; Goddard III, W. A. *J. Am. Chem. Soc.* **1978**, *100*, 5669.
(15) Yang, C. Y.; Johnson, K. H.; Holm, R. H.; Norman Jr., J. G. *J. Am. Chem. Soc.* **1975**, *97*, 6596.
(16) Norman Jr., J. G.; Jackels, S. C. *J. Am. Chem. Soc.* **1975**, *97*, 3833.
(17) Norman Jr., J. G.; Ryan, P. B.; Noodleman, L. *J. Am. Chem. Soc.* **1980**, *102*, 4279.
(18) Noodleman, L.; Norman Jr., J. G.; Osborne, J. H.; Aizman, A.; Case, D. A. *J. Am. Chem. Soc.* **1985**, *107*, 3418.
(19) Mouesca, J.-M.; Chen, J. L.; Noodleman, L.; Bashford, D.; Case, D. A. *J. Am. Chem. Soc.* **1994**, *116*, 11898.
(20) Adman, E.; Sieker, L. C.; Jensen, L. *J. Mol. Biol.* **1991**, *217*, 337.
(21) Day, M. W.; Hsu, B. T.; Joshua-Tor, L.; Park, J.-B.; Zhou, Z. H.; Adams, M. W. W.; Rees, D. C. *Protein Sci.* **1992**, *1*, 1494.

(22) Watenpaugh, K. D.; Sieker, L. C.; Jensen, L. H. *J. Mol. Chem.* **1980**, *138*, 615.
(23) Frey, M. W.; Sieker, L.; Payan, F.; Haser, R.; Bruschi, M.; Pepe, G.; LeGall, J. *J. Mol. Biol.* **1987**, *197*, 525.
(24) Swartz, P. D.; Beck, B. W.; Ichiye, T. *Biophys. J.* **1996**, *71*, 2958.
(25) Yelle, R. B.; Park, N. S.; Ichiye, T. *Proteins* **1995**, *22*, 154.
(26) Backes, G.; Mino, Y.; Loehr, T. M.; Meyer, T. E.; Cusanovich, M. A.; Sweeney, W. V.; Adman, E. T.; Sander-Loehr, J. *J. Am. Chem. Soc.* **1991**, *113*, 2055.
(27) Ziegler, T. *Chem. Rev.* **1991**, *91*, 651.
(28) Perez-Jorda, J. M.; Becke, A. D. *Chem. Phys. Lett.* **1995**, *233*, 134.
(29) Sim, F.; St-Amant, A.; Papai, I.; Salahub, D. R. *J. Am. Chem. Soc.* **1992**, *114*, 4391.
(30) Koerner, J. B.; Ichiye, T. Unpublished results.
(31) Werth, M. T.; Kurtz, J. D. M.; Howes, B. D.; Huynh, B. H. *Inorg. Chem.* **1989**, *28*, 1357.
(32) Hoffmann, R.; Lipscomb, W. N. *J. Chem. Phys.* **1962**, *37*, 2782.
(33) Ammeter, J. H.; Burgi, H.-B.; Thibeault, J. C.; Hoffmann, R. *J. Am. Chem. Soc.* **1978**, *100*, 3686.
(34) Hoffman, D. M.; Hoffmann, R.; Fisel, C. R. *J. Am. Chem. Soc.* **1982**, *104*, 3858.
(35) Watenpaugh, K. D.; Seiker, L. C.; Jensen, L. H. *J. Mol. Biol.* **1979**, *131*, 509.
(36) Phillips, W. D.; Poe, M.; Weiher, J. F.; McDonald, C. C. *Nature* **1970**, *227*, 574.
(37) Frisch, M. J.; Trucks, G. W.; Head-Gordon, M.; Gill, P. M. W.; Wong, M. W.; Foresman, J. B.; Johnson, B. G.; Schlegel, H. B.; Robb, M. A.; Replogle, E. S.; Gomperts, R.; Andres, J. L.; Raghavachari, K.; Binkley, J. S.; Gonzalez, C.; Martin, R. L.; Fox, D. J.; Defrees, D. J.; Baker, J.; Stewart, J. J. P.; Pople, J. A. *Gaussian 92, Revision A*; Gaussian Inc.: Pittsburgh, PA, 1992.
(38) Schmidt, M. W.; Baldridge, K. K.; Boatz, J. A.; Elbert, S. T.; Gordon, M. S.; Jensen, J. H.; Koseki, S.; Matsunaga, N.; Nguyen, K. A.; Su, S.; Windus, T. L.; Dupuis, M.; Montgomery, J. A. *J. Comput. Chem.* **1993**, *14*, 1347.
(39) Hay, P. J.; Wadt, W. R. *J. Chem. Phys.* **1985**, *82*, 299.
(40) Wadt, W. R.; Hay, P. J. *J. Chem. Phys.* **1985**, *82*, 284.
(41) Binkley, J. S.; Pople, J. A.; Hehre, W. J. *J. Am. Chem. Soc.* **1980**, *102*, 939.
(42) Collins, J. B.; Schleyer, P. v. R.; Binkley, J. S.; Pople, J. A. *J. Chem. Phys.* **1976**, *64*, 5142.
(43) Hehre, W. J.; Stewart, R. F.; Pople, J. A. *J. Chem. Phys.* **1969**, *51*, 2657.
(44) Wachters, A. J. H. *J. Chem. Phys.* **1970**, *52*, 1033.
(45) Rappe, A. K.; Smedley, T. A.; Goddard III, W. A. *J. Phys. Chem.* **1981**, *85*, 2607.
(46) Bach, R. D.; Su, M.-D.; Andres, J. L.; Schlegel, H. B. *J. Am. Chem. Soc.* **1993**, *115*, 8763.
(47) Turner, D. W.; Baker, A. P.; Brudle, C. R. *Molecular Photoelectron Spectroscopy*; Interscience: New York, 1970.
(48) Ohno, K. Ab-initio computations of metal−porphine complexes. In *Horizons of Quantum Chemistry*; Fukui, K., Pullman, B., Eds.; D. Reidel: Dortrecht, 1980; p 245.
(49) Dedieu, A.; Rohmer, M. M.; Veillard, A. Ab initio calculations of metalloporphyrins. In *Advances in Quantum Chemistry*; Lowdin, P. O., Ed.; Academic Press: New York, 1982; Vol. 16, p 43.
(50) Spackman, M. A. *J. Comput. Chem.* **1996**, *17*, 1.
(51) Spackman, M. A. *J. Chem. Phys.* **1986**, *85*, 6579. Value for Fe not obtained from this reference. Since there is a lack of comparative data for establishing the VDW radii of the transition metals, GAMESS approximates all of them as having a VDW radii of 1.8 Å.
(52) Breneman, C. M.; Wiberg, K. B. *J. Comput. Chem.* **1990**, *11*, 361.
(53) Calhourda, M. J.; Carrondo, M. A. A. F. d. C. T.; Dias, A. R.; Frazao, C. F.; Hursthouse, M. B.; Martinho Simoes, J. A.; Teixeira, C. *Inorg. Chem.* **1988**, *27*, 2513.
(54) Darensbourg, M. Y.; Silva, R.; Reibenspies, J.; Prout, C. K. *Organometallics* **1989**, *8*, 1315.
(55) Darensbourg, M. Y.; Bischoff, C. J.; Houliston, S. A.; Pala, M.; Reibenspies, J. *J. Am. Chem. Soc.* **1990**, *112*, 6905.
(56) Albright, T. A.; Burdett, J. K.; Whangbo, M.-H. *Orbital Interactions in Chemistry*; John Wiley and Sons: New York, 1985.
(57) These BSI optimized structures are similar to the BSII optimized structures given in Table 2. BSI results for **2** are as follows. Oxidized: Fe−$S_{1,2}$, 2.44 Å; Fe−$S_{3,4}$, 2.41 Å. Reduced: Fe−$S_{1,2}$, 2.61 Å; Fe−$S_{3,4}$, 2.56 Å. Oxidized: Fe−$S_{1,2}$−$C_{1,2}$, 113.6°; Fe−$S_{3,4}$−$C_{3,4}$, 101.6°. Reduced: Fe−$S_{1,2}$−$C_{1,2}$, 111.6°; Fe−$S_{3,4}$−$C_{3,4}$, 102.8°.
(58) Woods, R. J.; Khalil, M.; Pell, W.; Moffat, S. H.; Smith, J., V. H. *J. Comput. Chem.* **1990**, *11*, 297.
(59) Lane, R. W.; Ibers, J. A.; Frankel, R. B.; Papaefthymiou, G. C.; Holm, R. H. *J. Am. Chem. Soc.* **1977**, *99*, 84.
(60) Luthi, H. P.; Siegbahn, P. E. M.; Almlof, J.; Aegri Jr., K. F.; Heiberg, A. *Chem. Phys. Lett.* **1984**, *111*, 1.
(61) Taylor, T. E.; Hall, M. B. *Chem. Phys. Lett.* **1985**, *114*, 338.
(62) Reed, A. E.; Weinhold, F. *J. Am. Chem. Soc.* **1986**, *108*, 3586.
(63) Reed, A. E.; Schleyer, P. v. R. *J. Am. Chem. Soc.* **1990**, *112*, 1434.
(64) Magnusson, E. *J. Am. Chem. Soc.* **1990**, *112*, 7940.
(65) Chirlian, L. E.; Francl, M. M. *J. Comput. Chem.* **1987**, *8*, 894.
(66) Wiberg, K. B.; Rablen, P. R. *J. Comput. Chem.* **1993**, *14*, 1504.
(67) Bytheway, I.; Bacskay, G. B.; Hush, N. S. *J. Phys. Chem.* **1996**, *100*, 6023.
(68) Francl, M. M.; Carey, C.; Chirlian, L. E.; Gange, D. M. *J. Comput. Chem.* **1996**, *17*, 367.
(69) The charges from the DFT study are as follows: Oxidized: Fe, +0.813; S, −0.507; CH_3, +0.054. Reduced: Fe, +0.900; S, −0.708; CH_3, −0.017.
(70) Banci, L.; Bertini, I.; Carloni, P.; Luchinat, C.; Orioli, P. L. *J. Am. Chem. Soc.* **1992**, *114*, 10683.
(71) Jorgensen, W. L.; Swenson, C. J. *J. Am. Chem. Soc.* **1985**, *107*, 569.
(72) Simpson II, C. Q.; Hall, M. B. *New J. Chem.* **1991**, *15*, 763.